Supporting Information

Cyano-Functionalized Pyrazine: An Electron-Deficient Unit as Solid Additive Enables Binary Organic Solar Cells With 19.67% Efficiency

Lijun Tu,[a] Hao Wang,[a] Weixu Duan[b], Ruijie Ma,[c,*] Tao Jia,[d] Top Archie Dela Peña,[e,f] Yongmin Luo,[e] Jiaying Wu,[e] Mingjie Li,[f] Xiaomin Xia,[a] Siqi Wu,[a] Kai Chen,[b,*] Yue Wu,[g] Yulin Huang,[h] Kun Yang,[h] Gang Li,[c,*] and Yongqiang Shi[a,*]

[a] Key Laboratory of Functional Molecular Solids, Ministry of Education, and School of Chemistry and Materials Science, Anhui Normal University, Wuhu, Anhui 241002, China. E-mail: shiyq@ahnu.edu.cn

[b] Guangxi Key Lab of Processing for Nonferrous Metals and Featured Materials and Key lab of new Processing Technology for Nonferrous Metals and Materials, Ministry of Education; School of Resources, Environments and Materials, Guangxi University, Nanning 530004, China. Email: chenkai@gxu.edu.cn

[c] Department of Electrical and Electronic Engineering, Research Institute of Smart energy (RISE), Photonic Research Institute (PRI), The Hong Kong Polytechnic University, Hung Hum Kowloon, Hong Kong 999077, China
Email: ruijie.ma@polyu.edu.hk; gang.w.li@polyu.edu.hk

[d] School of Optoelectronic Engineering, School of Mechanical Engineering, Guangdong Polytechnic Normal University, Guangzhou, 510665 China.

[e]Advanced Materials Thrust, Function Hub, The Hong Kong University of Science and Technology, Nansha, Guangzhou, 511400 China

[f] Faculty of Science, Department of Applied Physics, The Hong Kong Polytechnic University, Kowloon, Hong Kong, 999077 P. R. China

[g] Laboratory of Advanced Optoelectronic Materials, Suzhou Key Laboratory of Novel Semiconductor-Optoelectronics Materials and Devices, College of Chemistry Chemical Engineering and Materials Science, Soochow University, Jiangsu, Suzhou 215123, China.

[h] State Key Laboratory of Chemo/Biosensing and Chemometrics, College of Chemistry and Chemical Engineering, Hunan University, Changsha 410082, China; Shenzhen Research Institute of Hunan University, Shenzhen 518000, China.

1. Materials and Methods.

All commercially available solvents, reagents, and chemicals were used as received without further purification unless otherwise stated. Anhydrous toluene was distilled from Na/benzophenone, and anhydrous triethylamine and acetonitrile were distilled from CaH_2 under argon. Unless otherwise stated, all operations and reactions were carried out under argon using standard Schlenk line techniques. ^{1}H and ^{13}C NMR spectra were recorded on a Bruker Ascend 400 and 500 MHz spectrometer, and the chemical shifts were referenced to residual protio-solvent signals. Differential scanning calorimetry (DSC) curves were recorded on Mettler STAR^{e} (TA Instrument) in nitrogen with a heating ramp of 10 ºC min^{-1}, and thermogravimetric analysis (TGA) curves were collected on Mettler STAR^{e} (TA Instrument). UV-vis absorption spectra were measured using a Shimadzu UV-2500 recording spectrophotometer. AFM measurements were obtained by using a Dimension Icon AFM (Bruker) in a tapping mode.

2. Materials Synthesis.

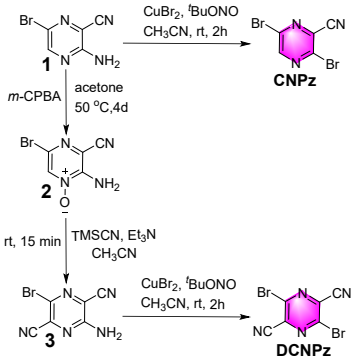

Scheme S1. Synthetic route to CNPz and DCNPz

Synthesis of 3,6-dibromopyrazine-2-carbonitrile (CNPz).

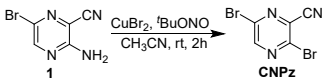

A solution of 1 (1.00 g, 5.02 mmol) in anhydrous acetonitrile (4 mL) was added to a stirred mixture of $CuBr_2$ (1.68 g, 7.54 mmol) and ^{t}BuONO (1.44 mL, 12.1 mmol) in anhydrous acetonitrile (10 mL) under argon. The mixture was stirred at room temperature for 2 h and then poured into 3M hydrochloric acid (50 mL) containing

sulfamic acid (0.73 g). The resulting solution was extracted with dichloromethane (3 × 20 mL), and the combined extracts were washed with brine, dried over sodium sulfate, filtered, and concentrated to dryness in vacuo. The mixture was purified by column chromatography on silica gel using with hexane-ethylacetate (3:1) to afford CNPz as a white solid (1.00 g, 76%). ^{1}H NMR ($CDCl_3$, 400 MHz) δ (ppm): 8.66 (s, 1H); ^{13}C NMR ($CDCl_3$, 100 MHz) δ (ppm): δ 150.12, 141.59, 138.89, 132.49, 113.53. HRMS: m/z (ESI) calculated for ($C_5H_2Br_2N_3$) $[M+H]^+$: 261.86100, found: 261.86037.

Synthesis of 2-Amino-5-bromo-3-cyanopyrazine 1-oxide (2).

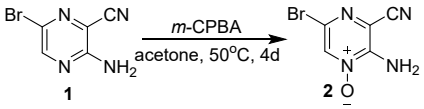

A solution of 1 (1.04 g, 5.02 mmol) and 3-chloroperbenzoic acid (70%, 1.61 g, 7.94 mmol) in acetone (40 mL) was stirred at 50 °C, and after 24 h another portion of 3-chloroperbenzoic acid (70%, 0.81 g, 3,97 mmol) was added. The mixture was further stirred at that temperature for 3 days, and then concentrated to dryness in vacuo. The residue was purified by flash-chromatography on silica gel using with hexane-ethyl acetate (3:1) to give 2 (0.70 g, 65%) ^{1}H NMR (400 MHz, DMSO) δ 8.87 (s, 1H), 8.16 (s, 2H); ^{13}C NMR (101 MHz, DMSO) δ 151.42, 136.29, 122.76, 114.80, 110.27.

Synthesis of 3-Amino-6-bromopyrazine-2,5-dicarbonitrile (3).

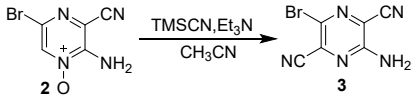

A solution of 2 (1.00 g, 4.65 mmol) in anhydrous acetonitrile (50 mL) containing distilled triethylamine (3.23 mL, 23.25 mmol) was placed in argon, and trimethylsilyl cyanide (2.19 mL, 17.67 mmol) was added dropwise. The mixture was stirred at room temperature for 15 min, and then ethanol (3 mL) was added. After stirring for 15 min, the mixture was concentrated to dryness in vacuo. The residue was purified by flash chromatography on silica gel using hexane-ethyl acetate (3:1) to afford 3 (0.49 g, 47%). ^{1}H NMR (400 MHz, DMSO) δ 8.10 (s, 2H); ^{13}C NMR (101 MHz, DMSO) δ 155.50, 133.05, 124.70, 115.30, 115.15, 114.54.

Synthesis of 3,6-Dibromopyrazine-2,5-dicarbonitrile (DCNPz).

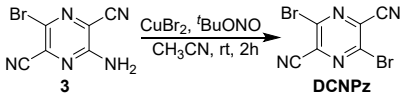

A solution of 3 (0.45 g, 2.0 mmol) in anhydrous acetonitrile (4 mL) was added to a stirred mixture of $CuBr_2$ (0.67 g, 3.0 mmol) and ^tBuONO (0.57 mL, 4.8 mmol) in anhydrous acetonitrile (10 mL) under argon. The mixture was stirred at room temperature for 2 h and then poured into 3M hydrochloric acid (20 mL) containing sulfamic acid (0.30 g). The resulting solution was extracted with dichloromethane (3 × 20 mL), and the combined extracts were washed with brine, dried over sodium sulfate, filtered, and concentrated to dryness in vacuo. The mixture was purified by column chromatography on silica gel using with hexane-ethylacetate (3:1) to afford DCNPz as an white solid (0.46 g, 80%). ^{13}C NMR (101 MHz, DMSO) δ 141.27, 134.33, 114.39. HRMS: m/z (ESI) calculated for (C6Br2N4) [M]+: 285.84952, found: 261.84963.

3. NMR Spectra of Monomers.

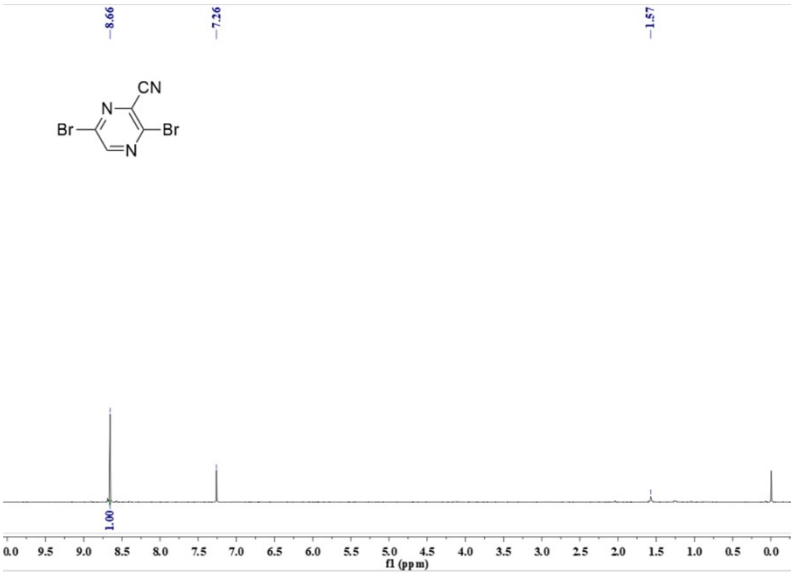

Figure S1. ^1H NMR spectrum of monomer **CNPz** (400 M, r.t., in $CDCl_3$).

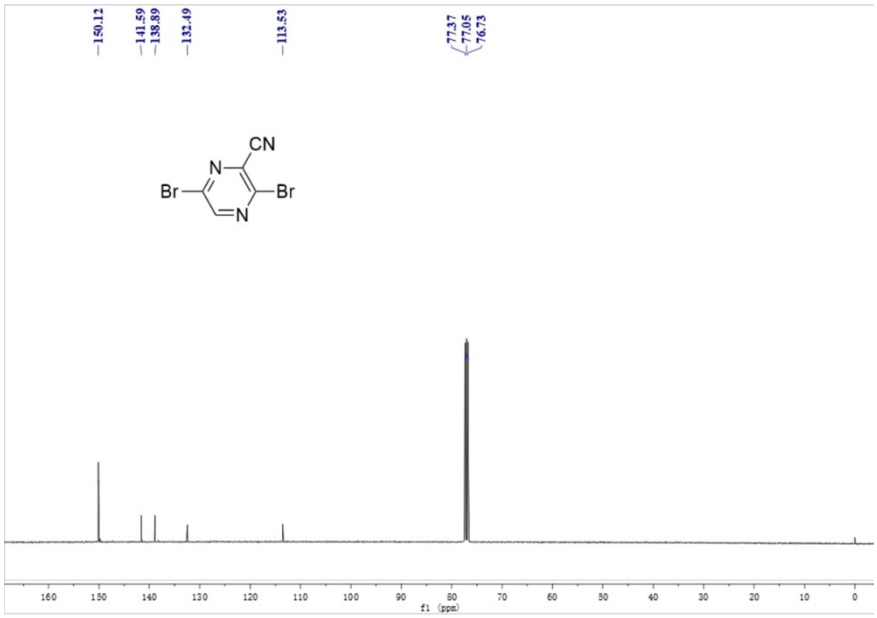

Figure S2. ^{13}C NMR spectrum of compound **CNPz** (100 M, r.t., in $CDCl_3$).

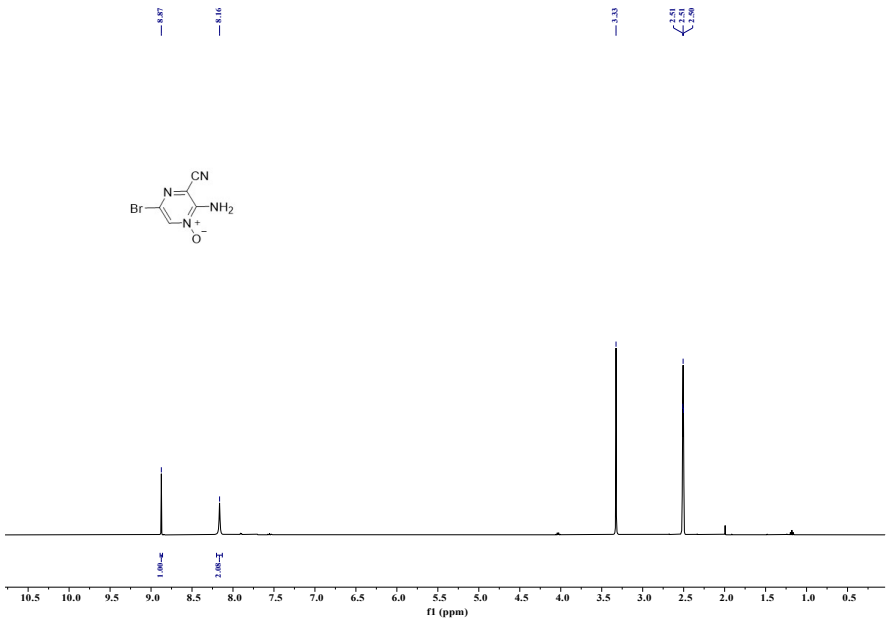

Figure S3. ^{1}H NMR spectrum of compound **2** (400 M, r.t., in DMSO).

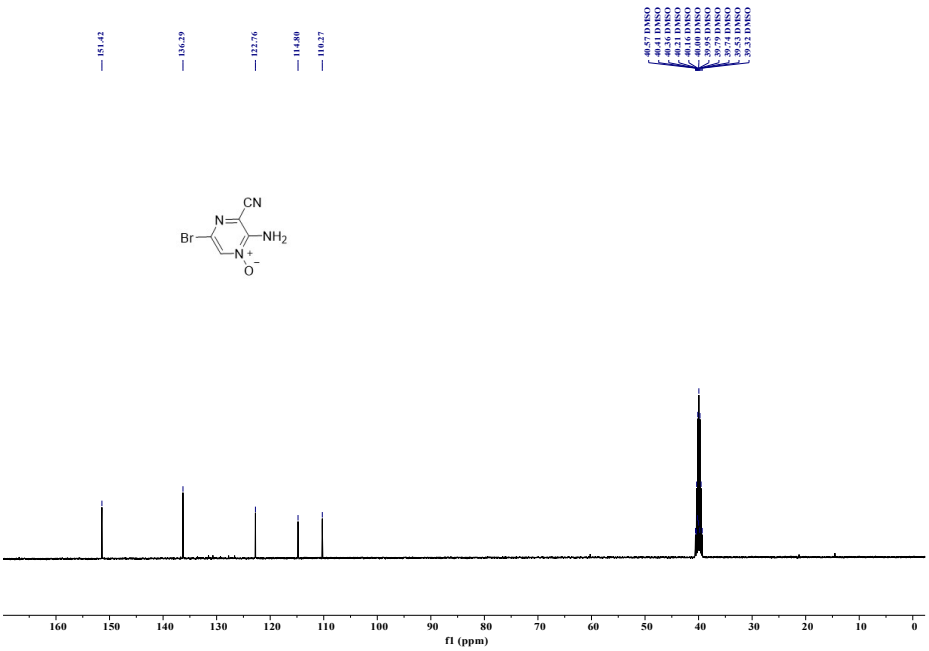

Figure S4. ^{13}C NMR spectrum of compound **2** (101 M, r.t., in DMSO).

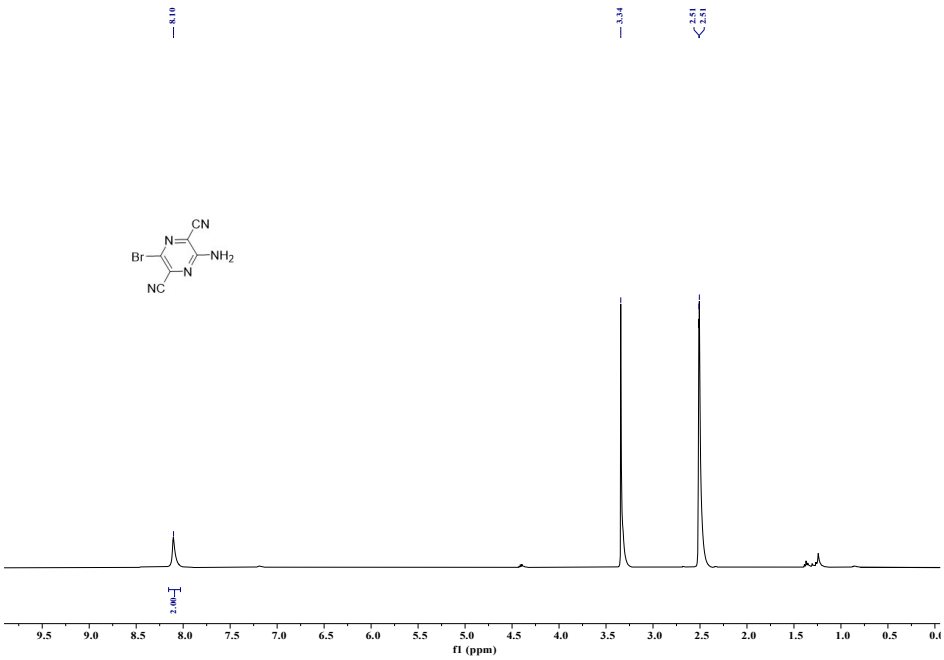

Figure S5. ^{1}H NMR spectrum of compound **3** (400 M, r.t., in DMSO).

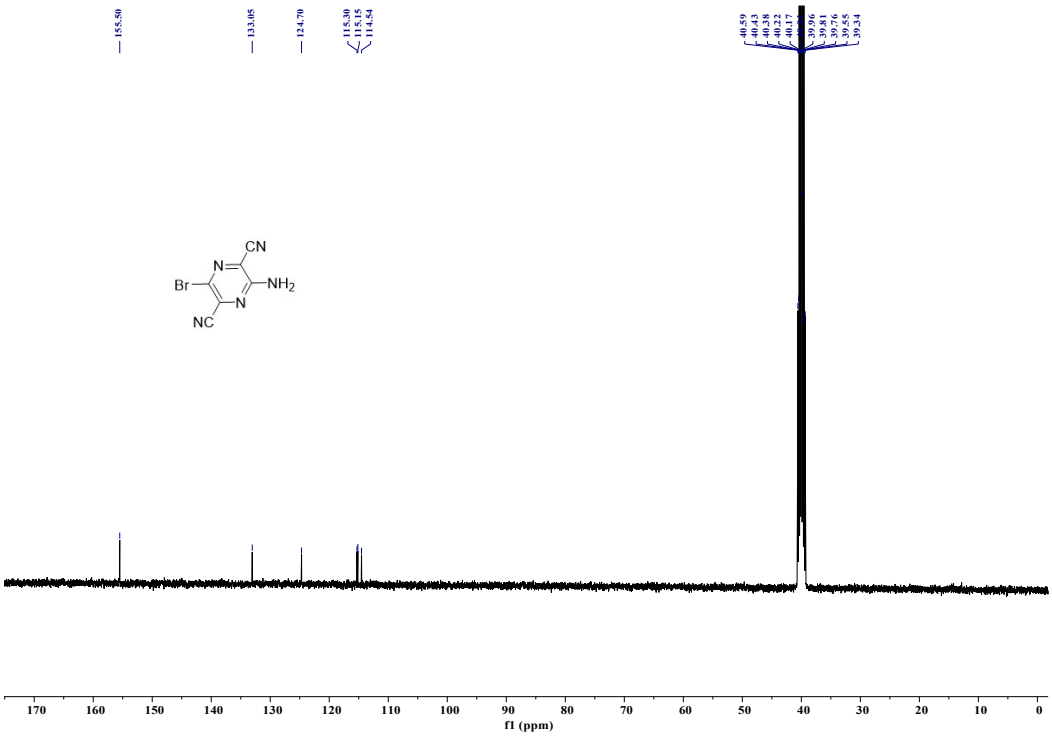

Figure S6. ^{13}C NMR spectrum of compound **3** (101 M, r.t., in DMSO).

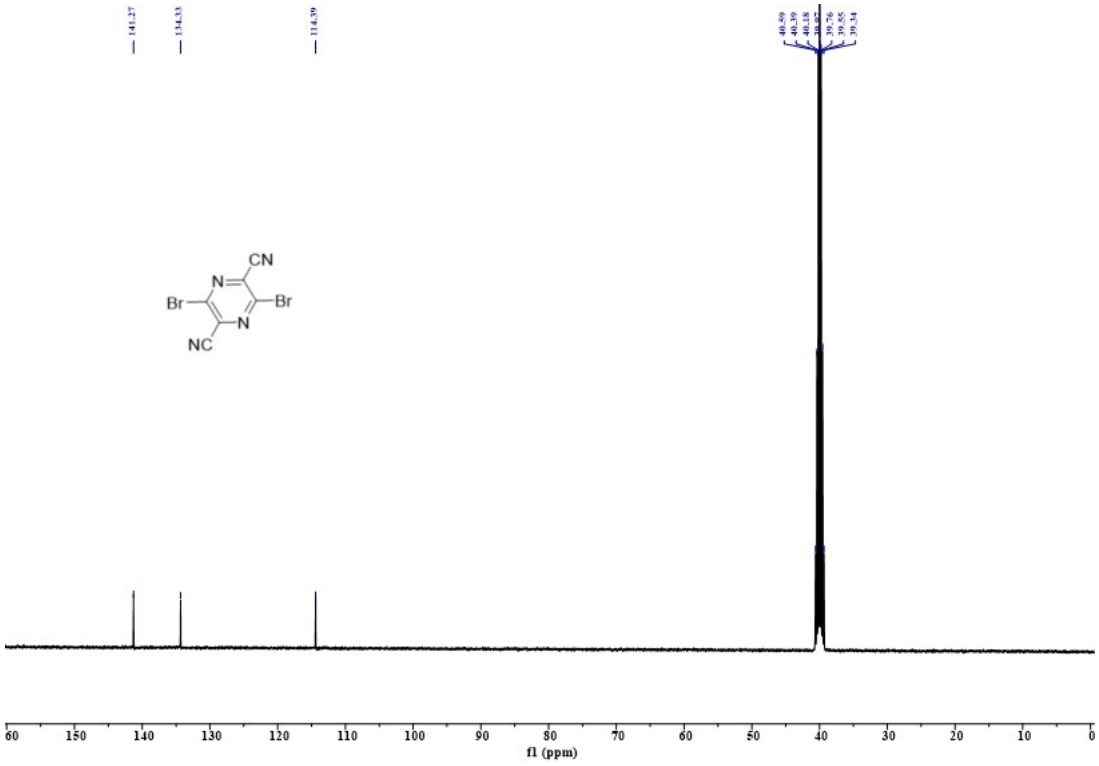

Figure S7. ^{13}C NMR spectrum of compound **DCNPz** (101 M, r.t., in DMSO).

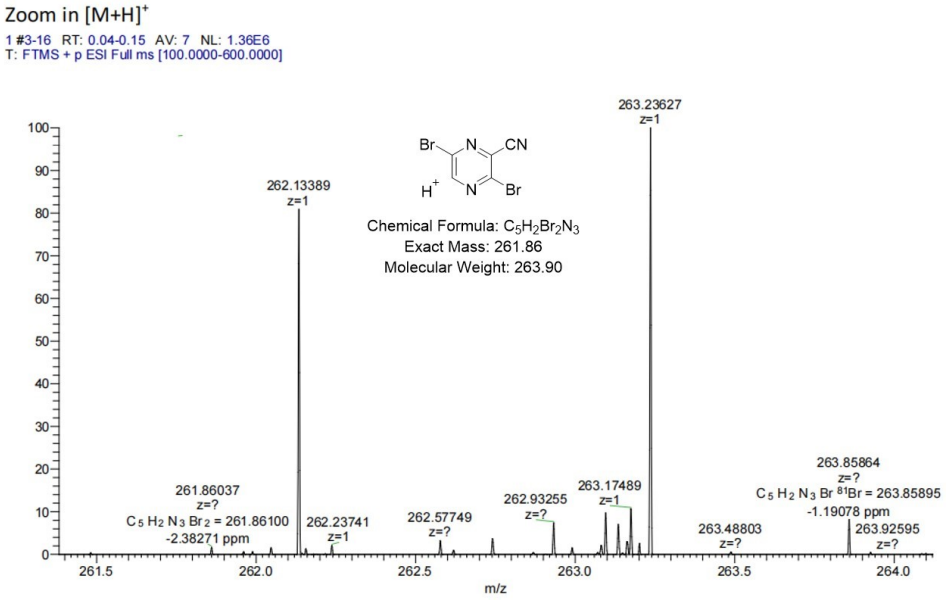

Figure S8. HRMS of CNPz.

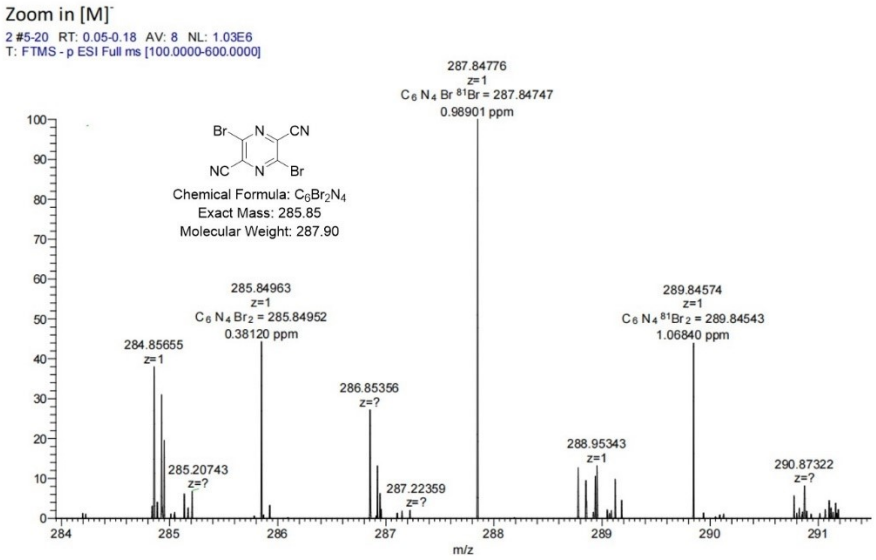

Figure S9. HRMS of DCNPz.

4. OSC fabrication and characterization

Solar cell fabrication and characterization

Solar cells were fabricated in a conventional device configuration of ITO/PEDOT:PSS-TA/active layers/PFN-Br/Ag. The ITO substrates (~94% transmittance) were first scrubbed by detergent and then sonicated with deionized water, acetone and isopropanol subsequently, and dried overnight in an oven. The glass substrates were

treated by UV-Ozone for 30 min before use. PEDOT:PSS-TA (Heraeus Clevios P VP AI 4083, doped by tyramine) was spin-cast onto the ITO substrates at 4000 rpm for 30 s, and then dried at 150 °C for 15 min in air. Afterwards, the substrates were transferred into a nitrogen filled glovebox where the active layer blend solutions has already been prepared inside. The PTQ10:m-BTP-PhC6 blend was dissolved in chloroform (8mg/mL 1:1.2) with 0.7 vol% 1-chloronaphthalene and 1mg/ml solid additives. The PTQ10 was provided by 1-Material Inc. (Cat. No.: OS0127; Lot# HW 5148; Mw = 126 KDa, Mn = 69 KDa), and the m-BTP-phC6 was bought from eFlexPV Inc.. The precursors were stirred at room temperature for 1 hour before using and cast onto prepared PEDOT:PSS films with 2300-2600 rpm (18 μL), followed by a thermal annealing on a 100 °C hotplate for 1 minute. PFN-Br thin layers were coated on the active layer with 3000 rpm (0.5 mg mL^{-1} in methanol), followed by the deposition of Ag (100 nm) (evaporated under 1×10^{-3} Pa through a shadow mask). The optimal active layer thickness measured by a Bruker Dektak XT stylus profilometer was about 100 nm. The current density-voltage (J-V) curves of devices were measured using a Keysight B2901A Source Meter in glove box under AM 1.5G (100 mW cm^{-2}) using an Enlitech solar simulator. The device contact area was 0.072 cm^2, device illuminated area during testing was 0.04 cm^2, which was determined by a mask. The EQE spectra were measured using a Solar Cell Spectral Response Measurement System QE-R3011 (Enlitech Co., Ltd.). The light intensity at each wavelength was calibrated using a standard monocrystalline Si photovoltaic cell.

SCLC Measurements

The electron and hole mobility were measured by using the method of space-charge limited current (SCLC) for electron-only devices with the structure of ITO/ZnO/active layer/PFN-Br/Ag and hole-only devices with the structure of ITO/PEDOT:PSS/active layers/MoO_x/Ag. The charge carrier mobility was determined by fitting the dark current to the model of a single carrier SCLC according to the equation: $J = 9\varepsilon_0\varepsilon_r\mu V^2/8d^3$, where J is the current density, d is the film thickness of the active layer, μ is the charge carrier

mobility, ε_r is the relative dielectric constant of the transport medium, and ε_0 is the permittivity of free space. $V = V_{app} - V_{bi}$, where V_{app} is the applied voltage, V_{bi} is the offset voltage. The charge carrier mobility was calculated from the slope of the $J^{1/2} \sim V$ curves. The thickness of target layer is well controlled identical to that of PV's active layer.

The Analysis of J_{ph} vs V_{eff} relationships

The definition of J_{ph} is the current density under illumination (J_L) minus the dark current density (J_D), and V_0 refers to the voltage value when $J_{ph} = 0$. Accordingly, $V_{eff} = V_0 - V_{appl}$, where V_{appl} represents applied voltage, has a clear meaning. Importantly, when V_{eff} reaches a high value (> 2V) it is normally believed that generated excitons are fully collected, in which J_{ph} is equal to saturated current density (J_{sat}). Then, we can calculate J_{SC}/J_{sat} and J_{max}/J_{sat} to describe exciton dissociation (η_{diss}) and charge collection (η_{coll}) efficiency. J_{max} is the J_{ph} at the maximal output point.

UV-vis and PL spectra fitting method

UV–vis and PL spectra are modelled as linear superpositions of basis spectra from individual absorbers:

$$A = \Sigma i\ bi \times i, \quad (1)$$

where A = f(E) is the decadic absorbance, bi = f(E) is the (unitless) basis spectrum of material i, which depends on the irradiated energy E, and si is the spectral weight (in units of eV). The index i ∈ {D, A} comprises the donor and acceptor materials, respectively, if applicable. The basis spectra for each material are given as linear superpositions of sub-bands whose shapes are given by hyperparameters that contain morphology information:

$$bi = \Sigma j\ bi,j\ (ai,j, wi,j, ci,j, dc,i,j, hi,j, ni,j), \quad (2)$$

where the index j ∈ {1o, 1a, 2, 3} comprises contributions from the three lowest energetic-allowed optical transitions. For j = 1, we distinguish between contributions from an ordered phase and an amorphous phase (suffixes 'o' and 'a', respectively). This picture has been shown to yield good results in P3HT, PM6 and Y6. We model electron–phonon coupling by assuming one effective vibronic progression as a

superposition of Gaussian bands of same width wi,j and fixed energy offset dci,j against the energy ci,j of the (0–0) vibronic transition57 for a given electronic transition and the individual spectral weight given by the Huang–Rhys factor, hi,j, of this effective progression. For donor polymers, we adopt the model of weak H aggregates ('Spano model') in which the (0–0) vibronic transition is suppressed by a factor ni,j with respect to the other vibronic transitions of the given progression. We use nonlinear regression (function curve_fit of the Python library scipy) to fit the experimental absorption spectra by tuning the hyperparameters in equation (2) and Penrose pseudo matrix inversion (using scipy function lsq_linear) to obtain the overall spectral weights in equation (1). However, because there is linear dependence between si and ai,j, we need to fix at least one of these parameters. Thus, we follow the convention that the ordered region of the lowest energetic electronic transition of each material has unity spectral weight:

$$a_{i,1o} \equiv 1 \qquad (3)$$

Furthermore, due to spectral congestion in the absorption spectra, we reduced the number of free hyperparameters by fixing $n_{D,1a} = n_{D,1o} = 0.5$, which is a typical value for donor polymers, and by fixing $n_{A,1a} = n_{A,1o} = 1$ because the acceptor systems of this work are dominated by strong J aggregates rather than weak H aggregates as would be required by the Spano model.

Transient Absorption Spectroscopy

Transient absorption spectroscopy (TAS) was measured with an amplified Ti:sapphire femtosecond laser (800 nm wavelength, 50 fs, 1 kHz repetition; Coherent Libra) and a Helios pump/probe setup (Ultrafast Systems). The 400 nm pump pulses with a pump fluence of 0.5 or < 3 μJ/cm^2 were obtained by frequency doubling the 800 nm fundamental regenerative amplifier output. The white-light continuum probe pulses were generated by focusing a small portion of the regenerative amplifier's fundamental 800 nm laser pulses into a 2 mm sapphire crystal.

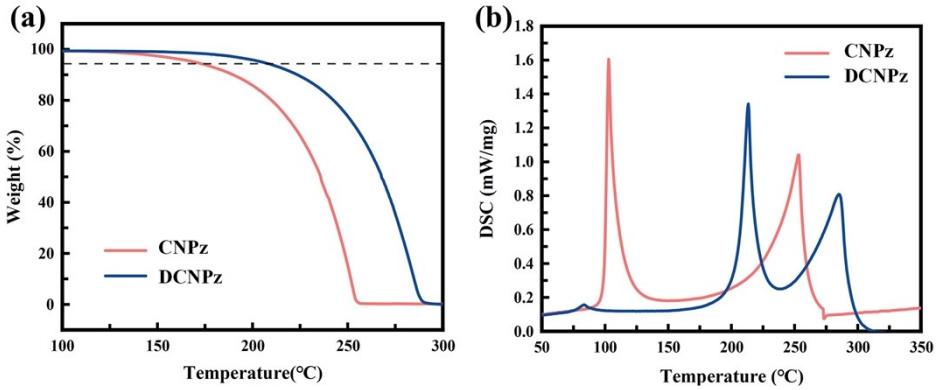

Figure S10. (a) Thermogravimetric analysis and (b) DSC thermograms of CNPz and DCNPz at a heating rate of 10 ºC min^{-1}.

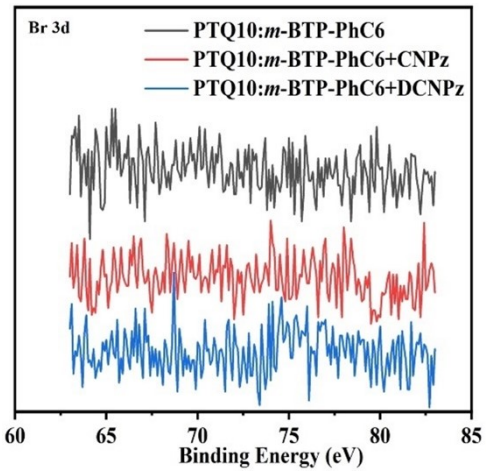

Figure S11. Br 3d XPS spectra of PTQ10:*m*-BTP-PhC6, CNPz-processed PTQ10:*m*-BTP-PhC6 system, and DCNPz-processed PTQ10:*m*-BTP-PhC6 system.

华南国家计量测试中心
广东省计量科学研究院
SOUTH CHINA NATIONAL CENTER OF METROLOGY
GUANGDONG INSTITUTE OF METROLOGY

校 准 证 书
CALIBRATION CERTIFICATE

证书编号 Certificate No. NYX202400115　　第 1 页，共 4 页 Page of

客户名称 Name of the Customer: 安徽师范大学/香港理工大学 Anhui Normal University/The Hong Kong Polytechnic University

联络信息 Contact Information: 中国，安徽，芜湖/中国，香港特别行政区，红磡 Wuhu, Anhui, China/Hung Hom, HKSAR, China

计量器具名称 Description: 有机太阳能电池 Organic solar cell

型号/规格 Model/Type: 有机太阳能电池 Organic solar cell

制造厂 Manufacturer: 安徽师范大学/香港理工大学

出厂编号 Serial No.: 1-3　　设备管理编号 Equipment No.: ----

接收日期 Date of Receipt: 2024 年 Y 03 月 M 20 日 D

结论 Conclusion: 见校准结果 Shown in the results of calibration

校准日期 Date of Calibration: 2024 年 Y 03 月 M 20 日 D

批 准 Authorized by 周军红

核 验 Reviewed by 周军红

校 准 Calibrated by 梅书刚

华南国家计量测试中心 证书专用章

扫一扫查真伪

实验室地址：广东省东莞市石排镇东园大道石牌段152号　　邮政编码：523343
电话：(8620)86594172 传真：(8620)86590743 投诉电话：(8620)36611242 E-mail：scm@scm.com.cn
Add: No.1,Miaobianwang Section, Dongyuan Road South, Shipai Town, Dongguan, Guangdong.
Post Code: 523343 Tel: (8620)86594172 Fax: (8620)86590743 Complaint Tel: (8620)36611242
证书真伪查询：www.scm.com.cn；cert.scm.com.cn Certificate AuthenticityIdentify: www.scm.com.cn; cert.scm.com.cn

华南国家计量测试中心
广东省计量科学研究院
SOUTH CHINA NATIONAL CENTER OF METROLOGY
GUANGDONG INSTITUTE OF METROLOGY

说　明

证书编号　NYX202400115
Certificate No.

DIRECTIONS

1. 本中心是国家市场监督管理总局在华南地区设立的国家法定计量检定机构，本中心的质量管理体系符合ISO/IEC 17025:2017标准的要求。
This laboratory is the National Legal Metrological Verification Institution in southern China set up by the State Administration for Market Regulation. The quality system is in accordance with ISO/IEC 17025:2017.

2. 本中心所出具的数据均可溯源至国家计量基准和/或国际单位制(SI)。
All data issued by this laboratory are traceable to national primary standards and/or International System of Units (SI).

3. 校准地点、环境条件：
Place and environmental conditions of the calibration:
地点　本院二基地A1-402　　温度　(25±2) ℃　　相对湿度　(50±5) %
Place　　Temperature　　R.H.

4. 本次校准的技术依据：
Reference documents for the calibration:
JJF1622-2017 太阳电池校准规范：光电性能　C.S.for Solar Cells: Photoelectric Properties

5. 本次校准所使用的主要计量标准器具：
Major standards of measurement used in the calibration:

设备名称/型号规格/测量范围 Name of Equipment /Model/Type/Range	编号 Serial No.	证书号/有效期/溯源单位 Certificate No./Due Date /Traceability to	计量特性 Metrological Characteristic
ABET 稳态太阳模拟器 1000W full spectrum solar simulator /SUN3000/(300～1300)W/m²	374	NYX202300746 /2024-12-28 /本中心	光谱匹配度：A级 辐照度不均匀性：A级 辐照度不稳性：A级
标准太阳能电池 Standard Solar Cell /RR_257_0/　Isc：(1～200)m A	13/01/2014	GXgf2023-03992 /2024-10-08 /中国计量院	U_{rel}=2.0%
标准源表 Standard Source Meter /2420/(0～60)V,(0～3)A	4051271	DBB202403401 /2025-02-26 /本中心	电压:U_{rel}=0.1%,电流:U_{rel}=0.1%(k=2) DCV:U_{rel}=0.1%,DCA:U_{rel}=0.1%(k=2)

华南国家计量测试中心
广东省计量科学研究院
SOUTH CHINA NATIONAL CENTER OF METROLOGY
GUANGDONG INSTITUTE OF METROLOGY

校 准 结 果
RESULTS OF CALIBRATION

证书编号 NYX202400115 Certificate No.　　原始记录号 NYX202400115 Record No.　　第 3 页,共 4 页 Page of

一、外观检查： 符合要求

Apparent Inspecti Pass.

二、测试条件： 温度(25±2)℃；辐照度1000W/m^2。

Test conditions: Temperature: (25±2)℃; Irradiance: 1000W/m^2.

三、电流-电压曲线：

The IV curve:

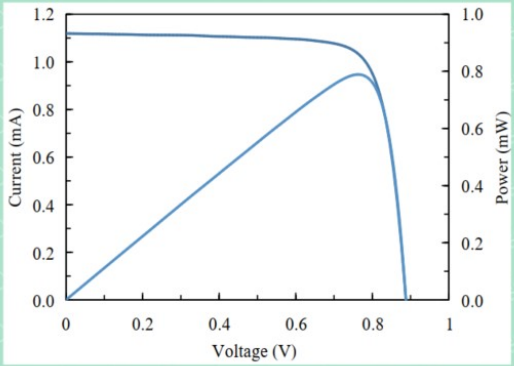

四、光电性能参数：

Results of photoelectric properties:

表1(Table 1)

短路电流密度J_{sc} Short ciruit current density	短路电流I_{sc} Short ciruit current	开路电压V_{oc} Open circuit voltage	填充因子FF Fill factor	最大功率P_m Maximum power	最佳工作电流I_m Optimum working current	最佳工作电压V_m Optimum working voltage	转换效率η Efficiency
mA/cm^2	mA	V	%	mW	mA	V	%
27.28	1.119	0.888	79.4	0.789	1.038	0.760	19.23

华南国家计量测试中心
广东省计量科学研究院
SOUTH CHINA NATIONAL CENTER OF METROLOGY
GUANGDONG INSTITUTE OF METROLOGY

校 准 结 果
RESULTS OF CALIBRATION

证书编号 NYX202400115 Certificate No.
原始记录号 NYX202400115 Record No.
第 4 页,共 4 页 Page of

说明：
Note:

1、电池有效面积数据为0.041 cm^2（有效面积基于金属掩模版面积）。
The effective area data of thecell is 0.041 cm^2 (Effective area based on a metal aperture mask).

2、本次测量结果的扩展不确定度为：开路电压V_{oc}：U_{rel}=1.2%，短路电流I_{sc}：U_{rel}=2.7%，最大功率P_{max}：U_{rel}=3.0%，(k=2)。
The expanded uncertainty of measuring results: V_{oc}: U_{rel}=1.2%, I_{sc}: U_{rel}=2.7%, P_{max}: U_{rel}=3.0%, (k=2).

3、本证书中给出的扩展不确定度依据JJF1059.1-2012《测量不确定度评定与表示》评定，由合成标准不确定度乘以包含概率约为95%时对应的包含因子k得到。
The expanded uncertainty given in this certificate is evaluated according to JJF 1059.1-2012"*Evaluation and Expression of Uncertainty in Measurement*",which is obtained by multiplying the combined standard uncertainty by the coverage factor k corresponding to the coverage probability of about 95%.

4、由于复校时间间隔的长短是由仪器的使用情况、使用者、仪器本身质量等诸因素所决定的，因此，送校单位可根据实际使用情况自主决定复校时间间隔。更换重要部件、维修或对仪器性能有怀疑时，应及时校准。
Since the calibration interval is determined by the use of the instrument,operation of the user, the quality of the instrument itself and other factors, the re-calibration date can decided by the user according to the actual situation. In case of replacement of important parts,maintenance or doubt on the performance of the instrument,it shall be calibrated in time.

Figure S12. Certified Efficiency of PTQ10:*m*-BTP-PhC6 binary system.

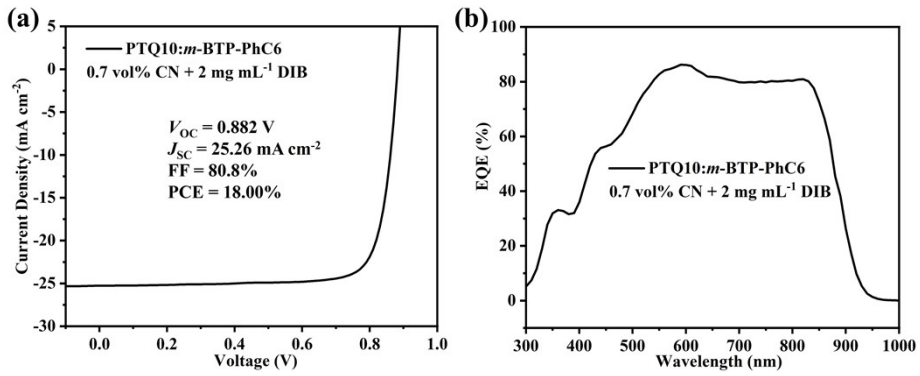

Figure S13. (a) *J-V* and (b) EQE curves of the OSCs based on PTQ10:*m*-BTP-PhC6 processed with DIB.

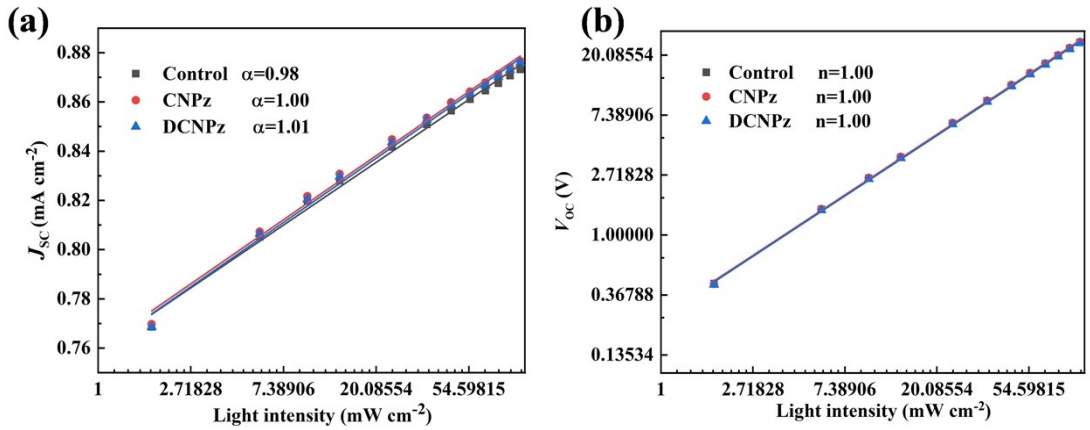

Figure S14. (a) J_{SC} versus light intensity, and (b) V_{OC} versus light intensity of the OSCs.

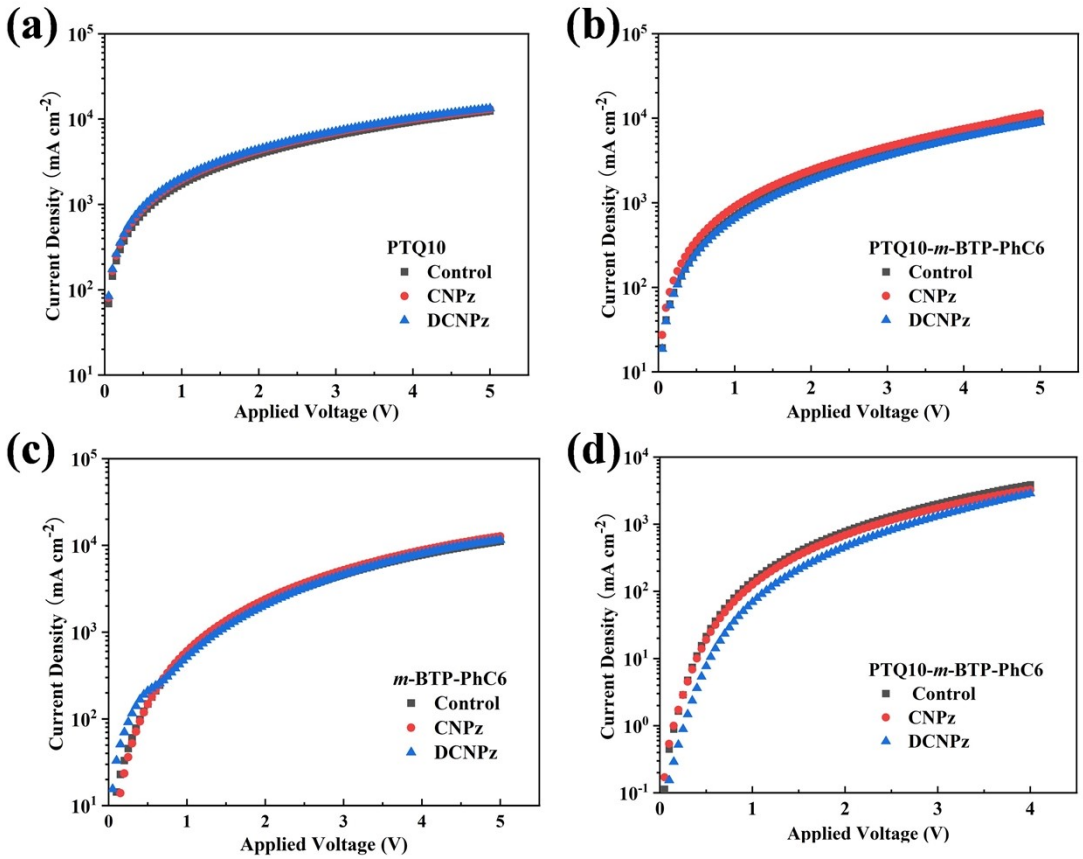

Figure S15. *J–V* characteristics of (a,b) hole-only devices with the structure of ITO/PEDOT:PSS/active layer/MoO_3/Ag and (c,d) electron-only devices with the structure of ITO/ZnO/active layer/PFN-Br/Al according to the SCLC model.

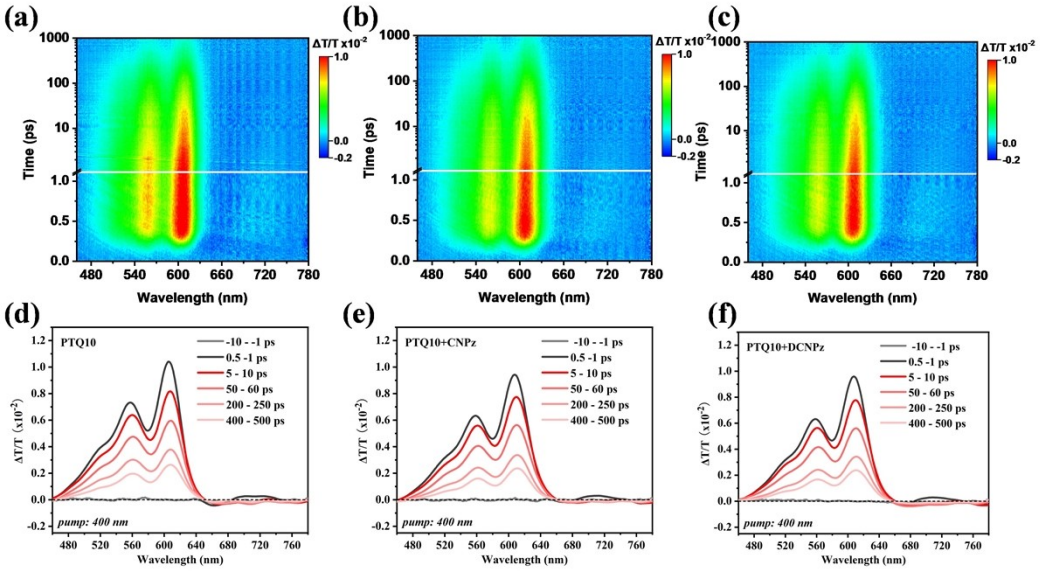

Figure S16. fs-TAS measurement of PTQ10 pure film without/with different additives: (a-c) pseudo 2D color plots. (d-f) Spectral line-cuts at indicated pump-probe delay times. The samples were excited using an 400 nm fs-laser with 3 uJ cm^{-2} fluence.

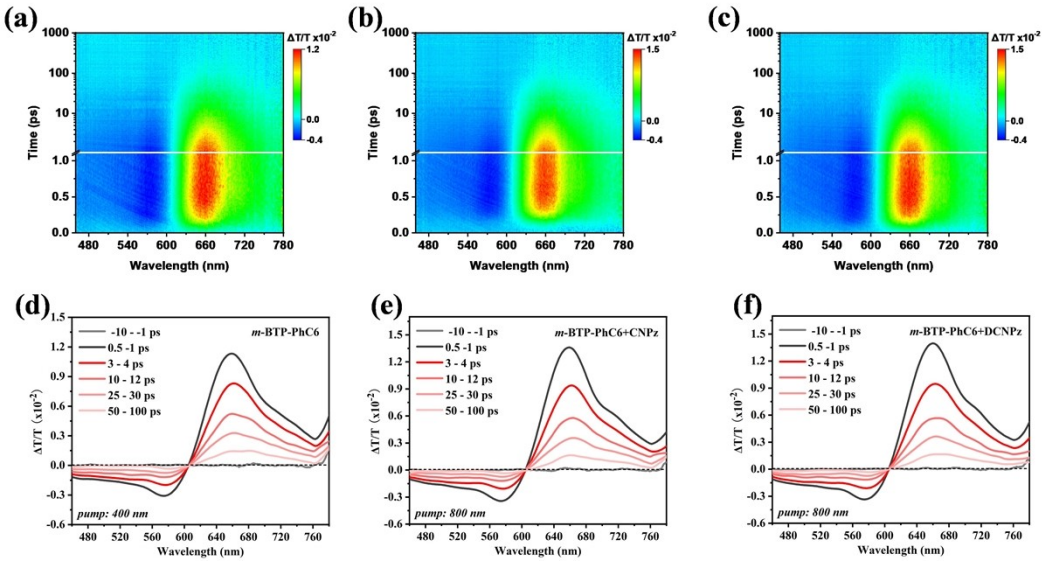

Figure S17. fs-TAS measurement of *m*-BTP-PhC6 pure film without/with different additives: (a-c) pseudo 2D color plots. (d-f) Spectral line-cuts at indicated pump-probe delay times. The samples were excited using an 800 nm fs-laser with 3 uJ cm^{-2} fluence.

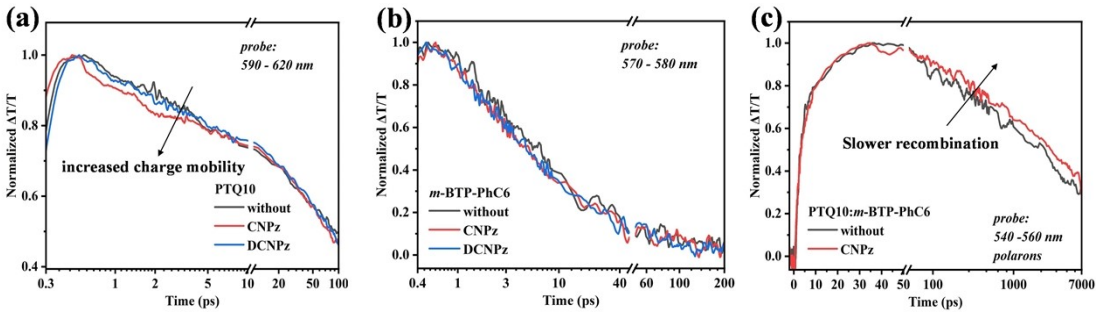

Figure S18. Carrier transfer kinetics analysis.

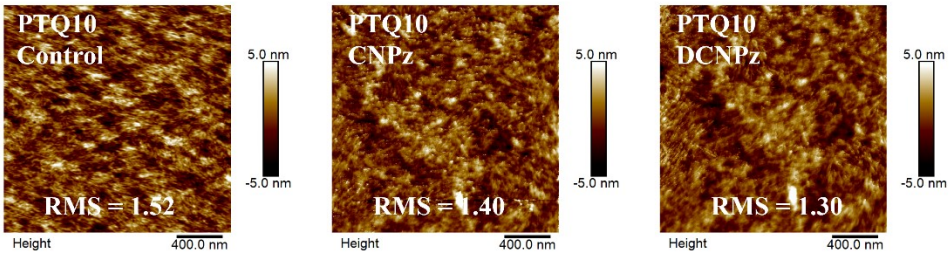

Figure S19. Atomic force microscopy (AFM) morphology images of PTQ10 without/with different solid additives.

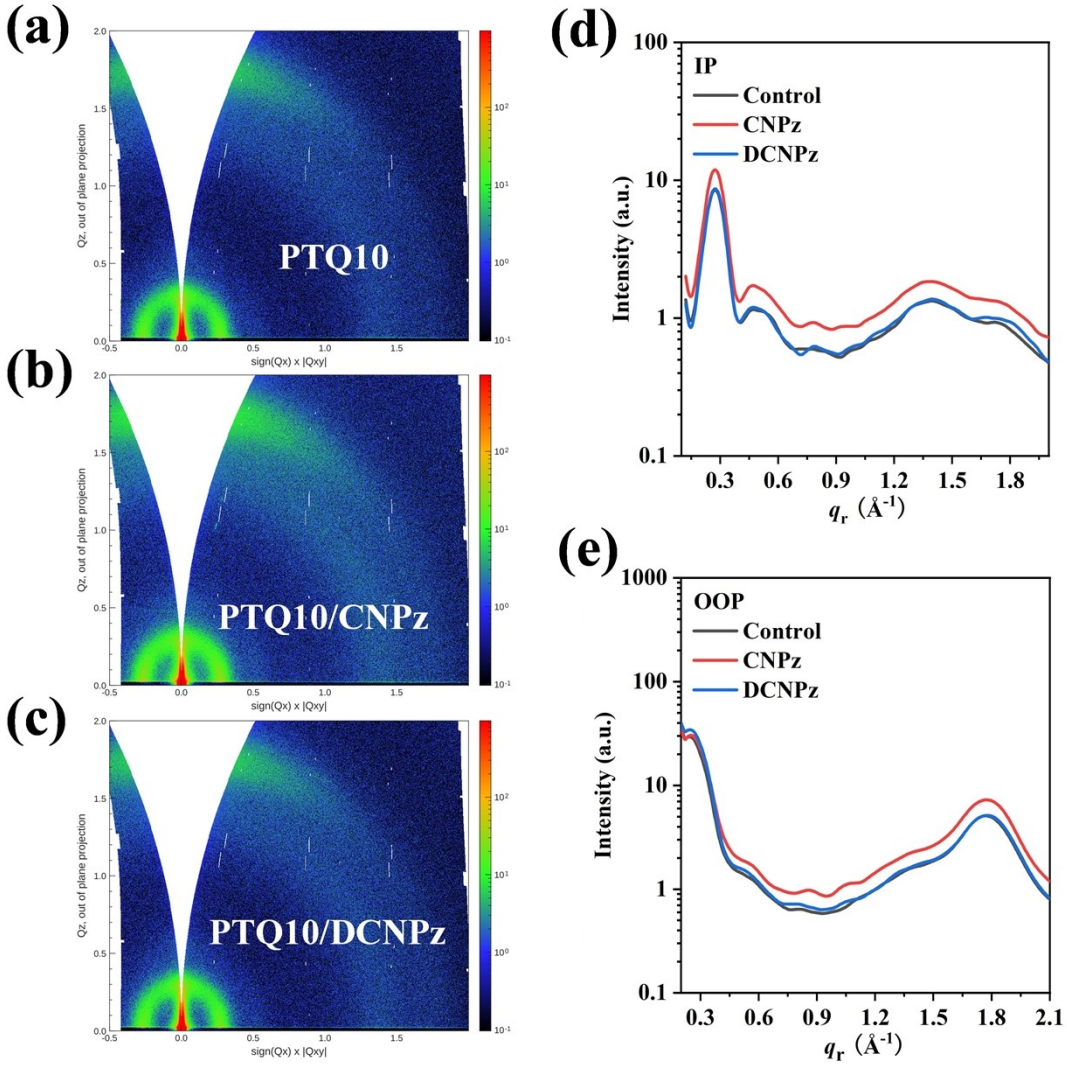

Figure S20. 2D GIWAXS patterns of PTQ10 pure film (a) control, (b) with CNPz additive and (c) with DCNPz additive. (d,e) The In-plane and Out-of-plane line cut of the 2D GIWAXS data.

Table S1. GIWAXS characteristics of the different additive-processed polymer donor PTQ10 film for q vector, d-spacing, and crystal coherence lengths (CCL) on IP direction.

Lamellar	q_{xy} (Å^{-1})	d-spacing (Å)	FWHM (Å^{-1})	CCL (Å)
Control	0.273	23.0	0.096	58.6
CNPz	0.273	23.0	0.096	58.8
DCNPz	0.274	23.0	0.097	58.3

π-π	q_{xy} (Å^{-1})	d-spacing (Å)	FWHM (Å^{-1})	CCL (Å)
Control	1.39; 1.73	4.51; 3.64	0.335; 0.233	16.9; 24.3
CNPz	1.39; 1.73	4.51; 3.64	0.352; 0.237	16.0; 23.9

DCNPz	1.39; 1.73	4.51; 3.64	0.311; 0.226	18.2; 25.0

Table S2. GIWAXS characteristics of the different additive-processed polymer donor PTQ10 film for q vector, d-spacing, and crystal coherence lengths (CCL) on OOP direction.

π-π	q_{xy} (Å^{-1})	d-spacing (Å)	FWHM (Å^{-1})	CCL (Å)
Control	1.48; 1.78	4.24; 3.54	0.337; 0.247	16.8; 22.9
CNPz	1.51; 1.78	4.17; 3.53	0.420; 0.252	13.5; 22.4
DCNPz	1.48; 1.78	4.24; 3.53	0.359; 0.252	15.7; 22.5

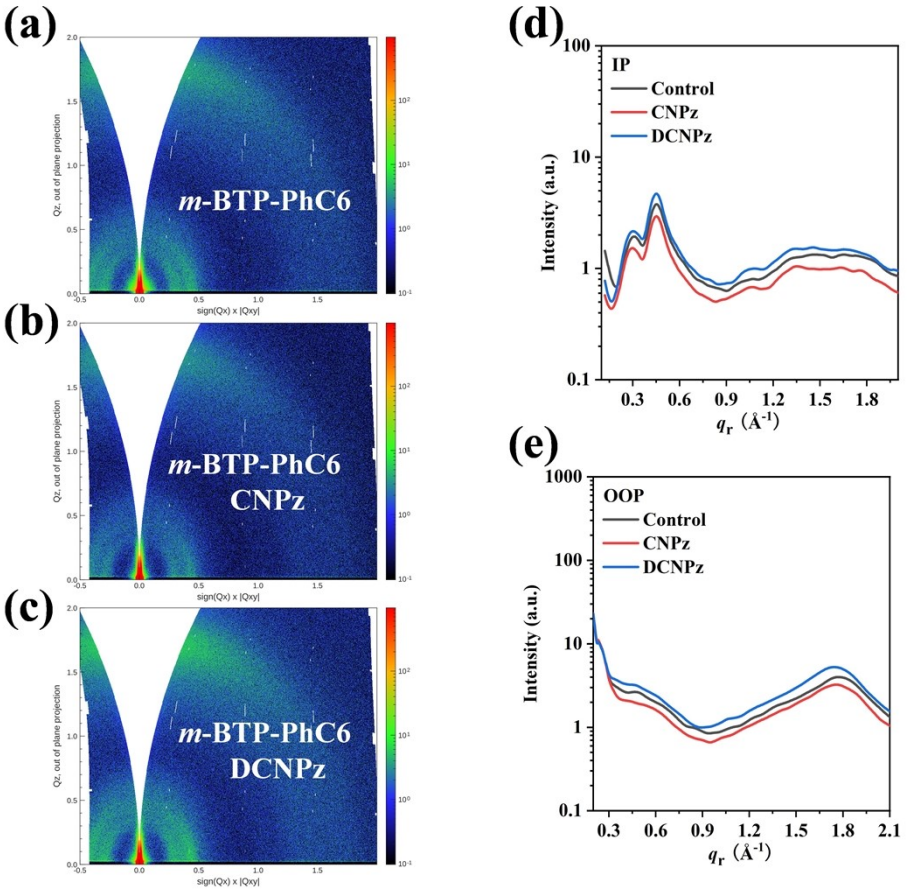

Figure S21. 2D GIWAXS patterns of *m*-BTP-PhC6 pure film (a) control, (b) with CNPz additive and (c) with DCNPz additive. (d,e) The In-plane and Out-of-plane line cut of the 2D GIWAXS data.

Table S3. GIWAXS characteristics of the different additive-processed *m*-BTP-PhC6 film for q vector, d-spacing, and crystal coherence lengths (CCL) on IP direction.

Lamellar	q_{xy} (Å^{-1})	d-spacing (Å)	FWHM (Å^{-1})	CCL (Å)
Control	0.309; 0.456	20.4; 13.8	0.060; 0.099	94.2; 57.4
CNPz	0.300; 0.454	20.9; 13.8	0.068; 0.100	83.2; 56.4
DCNPz	0.304; 0.453	20.7; 13.9	0.066; 0.098	86.2; 58.0

Table S4. GIWAXS characteristics of the different additive-processed *m*-BTP-PhC6 film for *q* vector, d-spacing, and crystal coherence lengths (CCL) on OOP direction.

π-π	q_{xy} (Å^{-1})	d-spacing (Å)	FWHM (Å^{-1})	CCL (Å)
Control	1.53; 1.79	4.10; 3.51	0.328; 0.285	17.3; 19.8
CNPz	1.46; 1.77	4.29; 3.55	0.346; 0.333	16.3; 17.0
DCNPz	1.51; 1.76	4.16; 3.57	0.330; 0.299	17.1; 18.9

Table S5. GIWAXS characteristics of the different additive-processed PTQ10:*m*-BTP-PhC6 film for *q* vector, d-spacing, and crystal coherence lengths (CCL) on IP direction.

Lamellar	q_{xy} (Å^{-1})	d-spacing (Å)	FWHM (Å^{-1})	CCL (Å)
Control	0.280; 0.452	22.4; 13.9	0.099; 0.135	57.1; 41.8
CNPz	0.280; 0.453	22.4; 13.9	0.099; 0.109	57.1; 51.7
DCNPz	0.278; 0.459	22.6; 13.7	0.099; 0.119	57.3; 47.7

π-π	q_{xy} (Å^{-1})	d-spacing (Å)	FWHM (Å^{-1})	CCL (Å)
Control	1.39; 1.73	4.51; 3.64	0.353; 0.232	16.0; 24.3
CNPz	1.40; 1.74	4.50; 3.61	0.353; 0.244	16.0; 23.2
DCNPz	1.39; 1.72	4.51; 3.65	0.340; 0.248	16.6; 22.8

Table S6. GIWAXS characteristics of the different additive-processed PTQ10:*m*-BTP-PhC6 film for *q* vector, d-spacing, and crystal coherence lengths (CCL) on OOP direction.

π-π	q_{xy} (Å^{-1})	d-spacing (Å)	FWHM (Å^{-1})	CCL (Å)
Control	1.52; 1.79	4.12; 3.52	0.339; 0.256	16.7; 22.0
CNPz	1.51; 1.79	4.17; 3.52	0.323; 0.261	17.5; 21.7
DCNPz	1.53; 1.80	4.11; 3.50	0.389; 0.261	14.5; 21.6

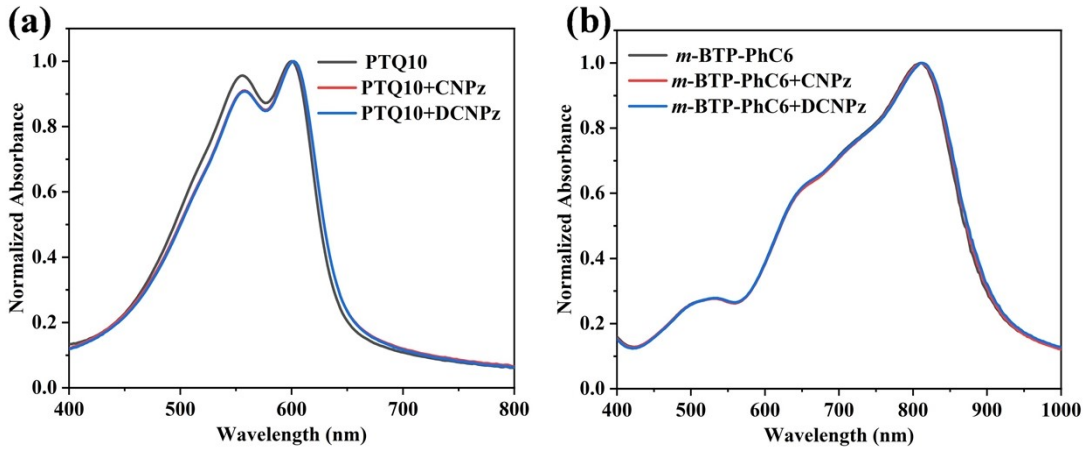

Figure S22. Absorption spectra of the (a) PTQ10 and (b) *m*-BTP-PhC6 without/with CNPz/DCNPz-processed films.

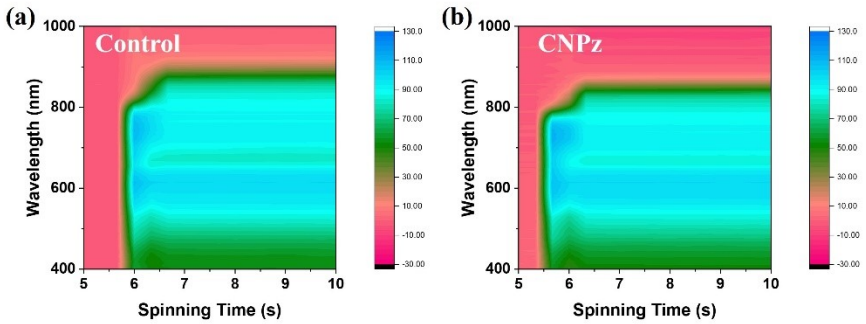

Figure S23. In situ UV/Vis absorption of PTQ10: *m*-BTP-PhC6 blend film. a) Control, b) CNPz-treated blend film, respectively.

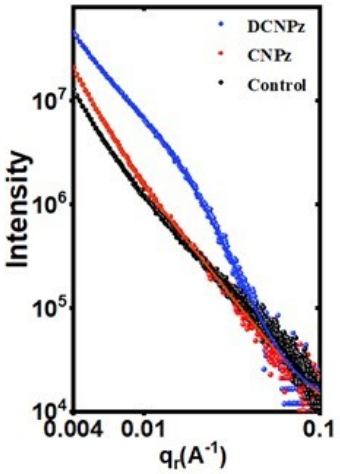

Figure S24. GISAXS intensity profiles and best fittings along the in-plane direction.

Table S7. The fitting Parameters Obtained from GISAXS 1D Profiles.

Condition	ξ (nm)	η (nm)	D	$2R_g$ (nm)
Control	41.8	8.7	2.2	32.6
CNPz	30.9	5.2	2.4	21
DCNPz	43.2	5.4	4.4	40

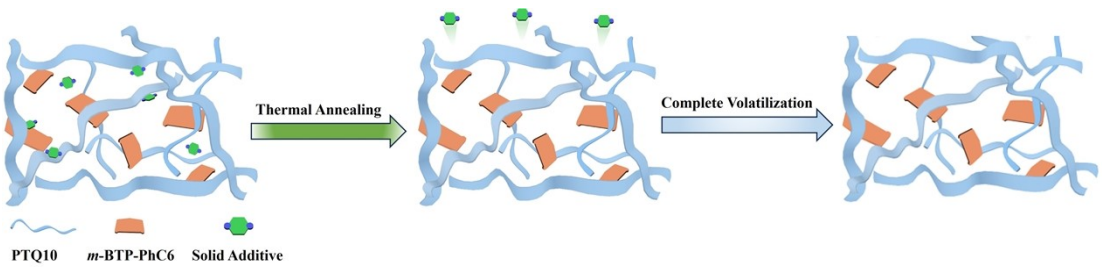

Figure S25. Schematic illustration for the working mechanism of solid additive in the film forming process.

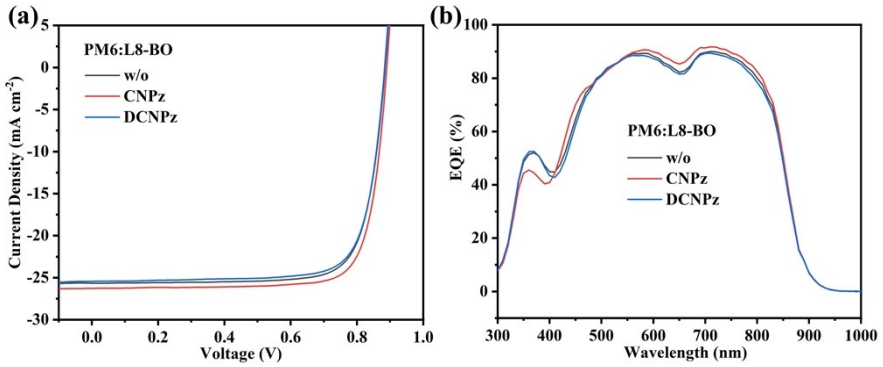

Figure S26. (a) *J-V* and (b) EQE curves for PM6:L8-BO system without/with solid additives.

Table S8. Photovoltaic parameters of the PM6:L8-BO system processed without or with different solid additives.

Solid Additive	V_{OC} (V)	J_{SC} (mA cm^{-2})	Cal. J_{SC} (mA cm^{-2})	FF (%)	PCE (%)
w/o	0.883	25.65	25.05	78.1	17.69
CNPz	0.890	26.27	25.51	79.3	18.56
DCNPz	0.885	25.43	24.75	77.6	17.46

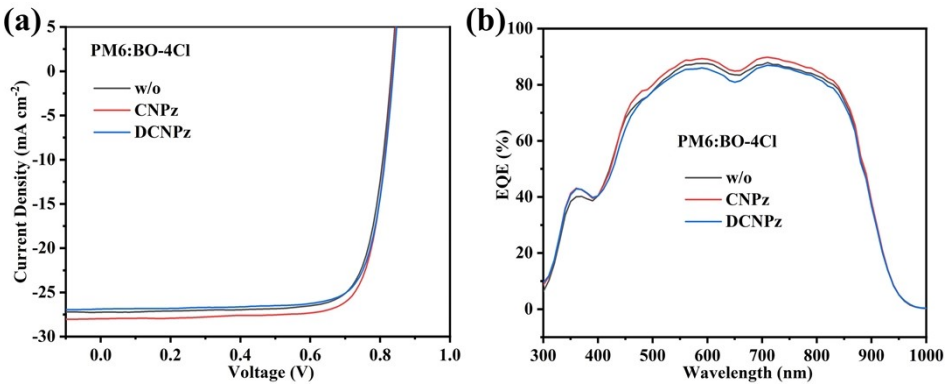

Figure S27. (a) *J-V* and (b) EQE curves for PM6:BO-4Cl system without/with solid additives.

Table S9. Photovoltaic parameters of the PM6:BO-4Cl system processed without or with different solid additives.

Solid Additive	V_{OC} (V)	J_{SC} (mA cm^{-2})	Cal. J_{SC} (mA cm^{-2})	FF (%)	PCE (%)
w/o	0.832	27.24	26.56	77.5	17.56
CNPz	0.835	27.97	27.11	78.3	18.29
DCNPz	0.835	26.88	26.13	76.7	17.22

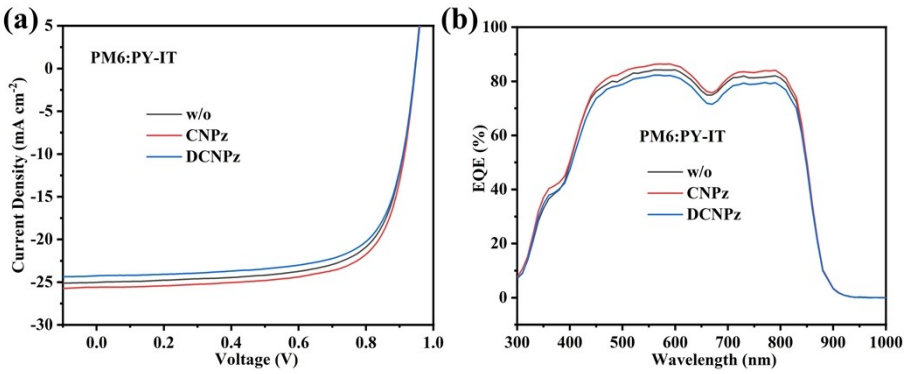

Figure S28. (a) *J-V* and (b) EQE curves for PM6:PY-IT system without/with solid additives.

Table S10. Photovoltaic parameters of the PM6:PY-IT system processed without or with different solid additives.

Solid Additive	V_{OC} (V)	J_{SC} (mA cm^{-2})	Cal. J_{SC} (mA cm^{-2})	FF (%)	PCE (%)
w/o	0.945	25.02	24.13	70.9	16.76
CNPz	0.946	25.59	24.65	72.0	17.43
DCNPz	0.946	24.25	23.38	70.8	16.24